

# RAMSES-CH: A New Chemodynamical Code for Cosmological Simulations

C.G. Few<sup>1\*</sup>, S. Courty<sup>2</sup>, B.K. Gibson<sup>1,3,4</sup>, D. Kawata<sup>5</sup>, F. Calura<sup>1,6</sup> and R. Teyssier<sup>7,8</sup>

<sup>1</sup>*Jeremiah Horrocks Institute, University of Central Lancashire, Preston, PR1 2HE, UK*

<sup>2</sup>*Université de Lyon; Université Lyon 1, Observatoire de Lyon, 9 avenue Charles André, Saint-Genis Laval, F-69230, France;*

*CNRS, UMR 5574, Centre de Recherche Astrophysique de Lyon; Ecole Normale Supérieure de Lyon*

<sup>3</sup>*Monash Centre for Astrophysics, School of Mathematical Sciences, Monash University, Clayton, VIC, 3800, Australia*

<sup>4</sup>*Department of Astronomy & Physics, Saint Mary's University, Halifax, Nova Scotia, B3H 3C3, Canada*

<sup>5</sup>*Mullard Space Science Laboratory, University College London, Holmbury St. Mary, RH5 6NT, United Kingdom*

<sup>6</sup>*Istituto Nazionale di Astrofisica, Osservatorio Astronomico di Bologna, Via Ranzani 1, I-40127, Bologna, Italy*

<sup>7</sup>*Institute for Theoretical Physics, University of Zürich, CH-8057, Zürich, Switzerland*

<sup>8</sup>*UMR AIM, CEA Saclay, 91191 Gif-sur-Yvette, France*

Submitted

## ABSTRACT

We present a new chemodynamical code – RAMSES-CH – for use in simulating the self-consistent evolution of chemical and hydrodynamical properties of galaxies within a fully cosmological framework. We build upon the adaptive mesh refinement code RAMSES, which includes a treatment of self-gravity, hydrodynamics, star formation, radiative cooling, and supernovae feedback, to trace the dominant isotopes of C, N, O, Ne, Mg, Si, and Fe. We include the contribution of Type Ia and II supernovae, in addition to low- and intermediate-mass asymptotic giant branch stars, relaxing the instantaneous recycling approximation. The new chemical evolution modules are highly flexible and portable, lending themselves to ready exploration of variations in the underpinning stellar and nuclear physics. We apply RAMSES-CH to the cosmological simulation of a typical  $L_*$  galaxy, demonstrating the successful recovery of the basic empirical constraints regarding,  $[\alpha/\text{Fe}]$ – $[\text{Fe}/\text{H}]$  and Type Ia/II supernovae rates.

**Key words:** galaxies: evolution – galaxies: formation – methods: N-body simulations

## 1 INTRODUCTION

The determination of elemental abundance patterns is one of the primary diagnostics of galaxy formation, with numerous spatial and temporal trends between age, kinematics, and chemistry guiding our insights into the underpinning physical processes. Observations of abundance ratios corroborate our understanding of the nuclear physics governing  $\alpha$ -element production, in that they are produced on shorter timescales than iron-peak elements (e.g. Carbon et al. 1987; Edvardsson et al. 1993; Reddy et al. 2006; Ramírez et al. 2007), as a consequence of the mass-dependent nuclear burning processes acting within the relevant progenitor stars. Galactic chemical evolution (CE) models are predicated upon a coupling of these elemental production sites/timescales with phenomenological (yet, empirically constrained) parameterisations of star formation and gas inflows/outflows. The resulting predicted abundance patterns can be compared directly with observations in order

to shed light on the formation and evolution of the system under study.

The formalism associated with the semi-numerical approach to galactic CE (e.g. Talbot & Arnett 1971; Pagel & Patchett 1975; Tinsley 1980; Matteucci & Francois 1989; Carigi 1994; Gibson 1997; Chiappini et al. 1997; Ramírez et al. 2007) is a powerful tool when applied to sub-grid CE treatments within fully hydrodynamical simulations. The inclusion of CE schemes has been achieved in a number of cosmological hydrodynamical codes (e.g. Lia et al. 2002; Valdarnini 2003; Kawata & Gibson 2003; Kobayashi 2004; Tornatore et al. 2004; Romeo et al. 2005; Martínez-Serrano et al. 2008; Oppenheimer & Davé 2008; Wiersma et al. 2009; Shen et al. 2010), each of which are based upon smoothed particle hydrodynamics (SPH). Key lessons can be learned from an examination of the role that CE plays in the physics of the interstellar medium. This is manifest in the metallicity-dependent radiative cooling rates of plasmas and their impact on the efficiency of metal transport throughout the disk and its consequent impact on stellar chemo-dynamics (Scannapieco et al. 2005). This impact upon turbulence-driven metal transport can be prob-

\* E-mail: cgfew@uclan.ac.uk

lematic, in light of known issues concerning the ability of conventional treatments of SPH to resolve the associated instabilities in certain regimes; such problems are ameliorated (though not entirely) by Eulerian approaches to fluid dynamics, including adaptive mesh refinement (AMR) schemes (e.g. O’Shea et al. 2005; Agertz et al. 2007; Tasker et al. 2008).

In its simplest form, interparticle ‘mixing’ of SPH particles does not occur, i.e. metal-rich and metal-poor gas particles may co-exist near each other without sharing/mixing of their associated metals. The impact of this lack of mixing is readily apparent in a galaxy simulation’s metallicity distribution function and age-metallicity relation, as well as the abundance ratio plane (e.g. Pilkington et al. 2012). The inclusion of turbulent mixing models within SPH remedies this lack of implicit diffusion (Shen et al. 2010), even if the associated diffusion coefficient is a necessary additional free parameter (albeit, informed by turbulence theory).

With the intention of providing a complementary (AMR) approach to extant (SPH) chemodynamical and semi-numerical CE models, we present what is, to our knowledge, the first cosmological AMR code which implements a temporally-resolved feedback and CE prescription. Written as a patch to the gravitational cosmological N-body and hydrodynamical code RAMSES, we now include the effects of Type II supernovae (SNeII), Type Ia supernovae (SNeIa), and low- to -intermediate-mass asymptotic giant branch (AGB) stars, both from an energetic and chemical perspective. Nucleosynthetic processes are accounted for as a function of progenitor mass and metallicity. The CE module is described in §2. The mechanics of marrying of this module to the AMR code RAMSES, leading to the self-consistent chemodynamical code RAMSES-CH, is outlined in §3. Finally, in §4, we present a demonstration of the ability of the code to reproduce basic observational constraints. We emphasise that this *Letter* is primarily a methodological description for coupling CE with AMR, and that future papers in this series will explore the response of RAMSES-CH to the various input parameters and assembly histories.

## 2 CHEMICAL EVOLUTION MODEL

The underlying CE model used to determine the relative rates of SNeII:SNeIa:AGB, and the associated chemical enrichment, for a stellar population governed by a given IMF, is generated prior to the simulation being run. The resulting look-up tables provide the SNeII, SNeIa, and isotopic return rates as a function of time for a range of Simple Stellar Population (SSP) metallicities. The code (provided as part of the RAMSES-CH patch) is flexible, allowing the user to readily modify relevant stellar physics, via the importation of different SNe and AGB yields, as well as the IMF.

For this first work, we have adopted a fairly standard/conservative CE model, employing a Kroupa (2001) IMF with stellar mass limits of 0.1 and 100  $M_{\odot}$ , respectively. We also used a SNIa delayed time distribution formalism similar to that presented in Kobayashi et al. (2000) and Kawata & Gibson (2003), with the simplification that the IMF slope for both the primaries and secondaries was taken to be identical. Stellar lifetimes were taken from Kodama & Arimoto (1997) and are dependent upon both mass and metallicity. The yields of SNeII progenitors

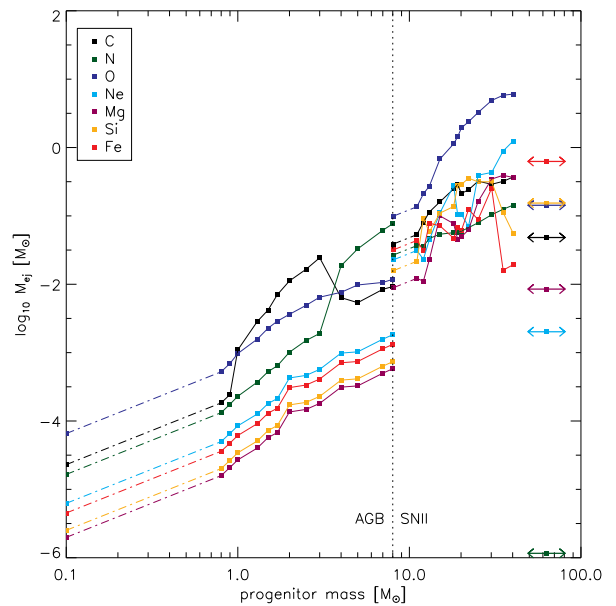


**Figure 1.** Mass of elements ejected by stars as a function of initial mass. Also shown are the abundances for a single SNeIa (horizontal arrows) for comparison (the position along the abscissa is arbitrary, chosen to avoid conflict with other data). The mass above which stars are considered to be SNeII progenitors is indicated at 8  $M_{\odot}$ . Data for AGB stars are taken from van den Hoek & Groenewegen (1997), SNeII from Woosley & Weaver (1995), and SNeIa from Iwamoto et al. (1999). Points connected by solid lines denote the original data, those connected by dot-dash lines show adopted extrapolations to lower masses. Extrapolations are linear and scaled to the mass of the progenitor star.

(11–40  $M_{\odot}$ ), for metallicities spanning Population III to solar, are from Woosley & Weaver (1995); for  $m > 30 M_{\odot}$ , we adopt the yields associated with the Model B explosion energies, after Timmes et al. (1995) and Kawata & Gibson (2003). Massive stars in the range 8–40  $M_{\odot}$  are assumed to explode as SNeII, where the yields in the range 8–11  $M_{\odot}$  are found by scaling the elemental mass fractions of the 11 $M_{\odot}$  stars with the progenitor mass. The same process is used to calculate the yields of stars down to 0.1 $M_{\odot}$  using the lowest mass (0.8 $M_{\odot}$ ) AGB star available in van den Hoek & Groenewegen (1997). The yields adopted are illustrated in Fig. 1.

As noted earlier, nucleosynthetic yields for SNeIa were taken from Iwamoto et al. (1999). In addition to the time constraints imposed by the mass range of the secondaries in SNeIa (binary) progenitors, Hachisu et al. (1999) also suggest the use of a metallicity ‘floor’ which suppresses the formation of low-metallicity ( $[Fe/H] < -1.1$ ) SNIa progenitors. In light of the ongoing controversy regarding this putative metallicity floor, we have adopted the conventional assumption that low-metallicity binaries are capable of forming SNeIa progenitors. These SNeIa yields are also noted in Fig. 1 by the horizontal arrows.

The time evolution of the isotopic ejection rate (per unit mass) from an SSP is shown in Fig. 2. The RAMSES-CH chemical evolution model generates a family of such ejection rates for any combination of yield compilation and initial

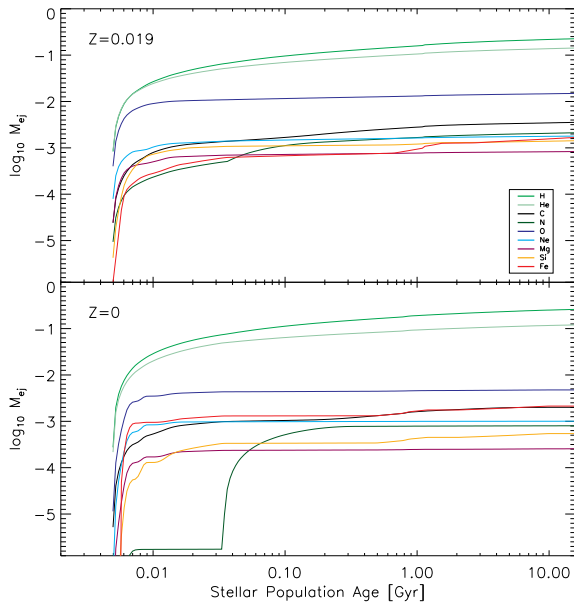


**Figure 2.** Ejection rate of dominant elemental isotopes, per unit stellar mass, as a function of age for a Kroupa (2001) IMF. The upper and lower panels correspond to solar and Population III metallicity simple stellar populations respectively.

mass function. We have chosen to simply show the impact of the choice of one conservative combination of parameters. This should not be construed as implying that this combination is necessarily the best or unique pairing; it is simply chosen to demonstrate the efficacy of the methodology.

### 3 RAMSES-CH

We have introduced the CE prescription into the v3.07 public release version of RAMSES (Teyssier 2002). Prior to these enhancements, RAMSES tracked the total gas metallicity ( $Z$ ), under the assumption of the instantaneous recycling approximation and treating  $Z$  as a passive scalar advected by the hydrodynamical flow. Our new chemodynamical version (RAMSES-CH) also employs passive scalars in the tracking of the dominant isotopes of H, C, N, O, Mg, Ne, Si, and Fe, and the chemical composition of the gas from which the stellar particles form is ‘tagged’ onto the new particles. As described by Dubois & Teyssier (2008), star particles are created in the high-density gas ( $\rho_{gas} > \rho_{th}$ ) and spawned by a random Poisson process following a rate given by  $\dot{\rho}_* = \epsilon_* \rho_{gas} / t_{ff}$ , where  $t_{ff}$  is the local free-fall time of the gas,  $(3\pi/32G\rho_{gas})^{1/2}$ , and  $\epsilon_*$  the star formation efficiency. Each stellar particle enriches the surrounding interstellar medium (ISM) according to its individual chemical history recorded in the look-up tables described in §2, depending upon the particle’s initial mass and metallicity. Chemical enrichment and feedback processes are treated simultaneously through a kinetic feedback mode. While we could apply kinetic feedback to all the stellar populations, we do so only to those stellar populations that include SNeII events. A thermal feedback mode is used when the stellar population ages and enters an AGB and SNIa ‘phases’. The kinetic feedback mode aims at reproducing those expanding gas flows gener-

ated by the collective explosions of massive stars. At each time-step, density, momentum, energy, and metals are deposited into all gas cells situated within a feedback-‘sphere’ of a user-specified radius centered upon the young star particles. We set up our SNeII feedback-sphere radius to 2 grid cells. The velocity of the entrained gas, linearly interpolated with the radius, is given by the number of SNeII events, the energy generated by each event  $\epsilon_{SN} E_{SN}$  ( $\epsilon_{SN}$  being the efficiency with which the energy  $E_{SN} = 10^{51}$  erg couples to the surrounding ISM), and the total amount of gas to be entrained by the bubble. The entrained gas includes the gas released/ejected during the SNeII events as well as the gas swept up by the bubble (Dubois & Devriendt, private comm.). This latter component is parametrized as  $f_w$  times the ejected gas mass ( $f_w = 10$  in this work, corresponding to a mass loading factor of  $\eta_w = 1$  for a standard run with a massive star fraction of 10%). The galactic outflow scheme just described is not applied for the SNIa events and when the stellar population enters an AGB and/or SNIa phase, feedback processes and chemical enrichment are handled ‘locally’ (thermally) and confined to the gas cell within which the stellar particle sits. The feedback algorithm is simplified by this approximation; future developments of the code will include kinetic SNIa feedback.

This new chemodynamical version of RAMSES was then applied in the generation of a multi-resolved, cosmological simulation of a late-type disk galaxy (henceforth called, 109-CH) with a virial mass of  $7.1 \times 10^{11} M_\odot$ , whose initial conditions match those outlined in an earlier study (Sánchez-Blázquez et al. 2009). To remind the reader, the box size for this run was  $L=20 h^{-1}$  Mpc, with a dark matter particle mass of  $6 \times 10^6 M_\odot$  in the most refined region. The spatial resolution, kept roughly constant in physical size during the simulation, reaches  $L/2^{lmax}=436$  pc at  $z=0$ , with  $lmax=16$  levels of refinement. For this resolution, we choose a star formation density threshold  $\rho_{th}$  corresponding to  $0.3 \text{ cm}^{-3}$  and an efficiency of 1%. The same SNe energy coupling efficiency of  $\epsilon_{SN} = 1$  is assumed for both SNeII and SNeIa. A polytropic equation of state  $T = T_{th}(\rho/\rho_{th})^{\gamma-1}$  is used in the high-density areas with a temperature threshold of 2900 K and a polytropic index  $\gamma=2$ , allowing the Jeans length to be resolved by more than 4 cells at all times. Note that our feedback parameter choices are suitable for the implementation described here at resolutions of 100–500pc.

### 4 CHEMODYNAMICS OF AN $L_*$ GALAXY

We introduce this new grid-based chemodynamical tool to the community. We now demonstrate the efficacy of RAMSES-CH through a presentation of the chemical properties of 109-CH. Future papers in this series will extend beyond this initial demonstration into a comprehensive chemical tagging and chemodynamical exploration of a suite of higher-resolution cosmological disks spanning a range of environments and assembly histories, realisations of which are described in Pilkington et al. (2012).

The first metric to consider when introducing SNeII and SNeIa in parallel with a relaxation of the instantaneous recycling approximation is the predicted supernovae rates and a comparison with empirical constraints. We show the time evolution of these rates in Fig. 3. For 109-CH, a present-day SNeIa rate of 0.131 SNUm (SNe per century

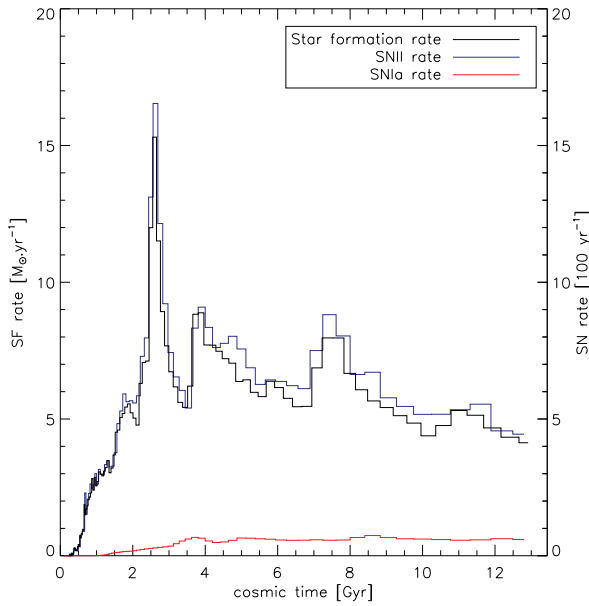


**Figure 3.** The star formation rate for 109-CH is shown in black (refer to the left-hand ordinate) and the corresponding SNeII and SNeIa rates are shown (refer to the right-hand ordinate) in blue and red, respectively. Note that the SNeII rate is not precisely proportional to the star formation rate as would be the case for data simulated using the “standard” version of RAMSES. The SNeII rate at each time is now dependant on the star formation rate of past as well as present time-steps.

per  $10^{10}M_{\odot}$  stellar mass) was found, and a SNeII rate of 0.959 SNUm. Both the absolute values and SNeII:SNeIa ratio ( $\sim 7$ ) are consistent with those found by Mannucci et al. (2008) for field Sbc/d galaxies:  $0.140^{+0.045}_{-0.035}$  SNUm for SNeIa and  $0.652^{+0.164}_{-0.134}$  SNUm for SNeII.

Moving beyond the SNe rates, the abundance ratios of readily observed elements are regularly employed to constrain the timescales of star formation, and therefore both feedback and fundamental nucleosynthesis. The recovery of empirical trends found locally in the solar neighbourhood is a necessity for any CE model. Such observations demonstrate a clear correlation between  $\alpha$ -element and iron abundances, in the sense of their being an  $\alpha$ -enhanced plateau at lower metallicities (below, say,  $[\text{Fe}/\text{H}] \sim -0.7$ ) with a systematic decline to solar values, at higher metallicities (e.g. Edvardsson et al. 1993; Gratton et al. 2003; Reddy et al. 2003; Cayrel et al. 2004; Bensby et al. 2005; Reddy et al. 2006). This empirical behaviour in  $[\alpha/\text{Fe}] - [\text{Fe}/\text{H}]$  can be seen in Fig. 4, where, in this case, we are showing the observational trends for  $[\text{O}/\text{Fe}]$  vs  $[\text{Fe}/\text{H}]$ . Also shown in Fig. 4 is the same distribution of  $[\text{O}/\text{Fe}] - [\text{Fe}/\text{H}]$  for the star particles at redshift  $z=0$  within an analogous ‘solar neighbourhood’ for the simulated disk 109-CH. We should emphasise that the solar normalisation employed for both simulated and observed data is that of Anders & Grevesse (1989).

A rigorous analysis of how the choice of SNeII, SNeIa, and AGB yields, in addition to the IMF and SNeIa progenitor model impact upon the chemodynamical evolution is left to future papers in this series, but it should be clear that even with this first ‘test’, the qualitative chemical properties are not inconsistent with observations of the

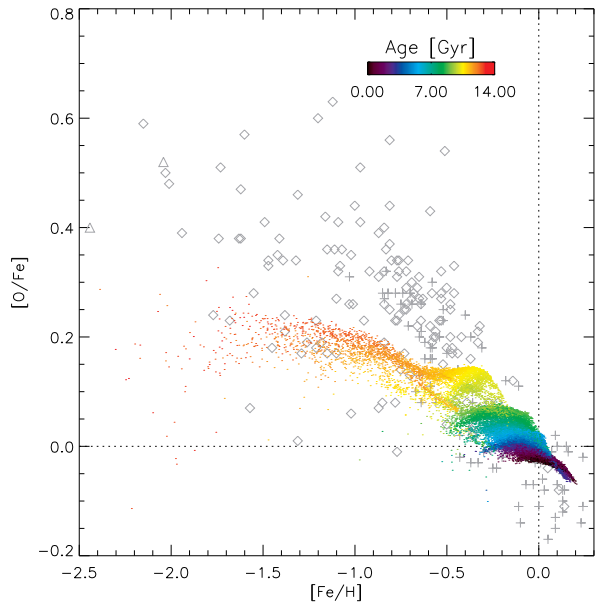


**Figure 4.** Abundance ratios of stars in a disk region of galactocentric radius between 5 and 11 kpc and within 3 kpc of the disk plane. Particles are coloured according to their age. Observational data is plotted in grey, triangles are very metal-poor stars from Cayrel et al. (2004), diamonds are thick disk and halo stars from Gratton et al. (2003), pluses are disk dwarf stars from Edvardsson et al. (1993). All data has been normalised to the solar abundance determination of Anders & Grevesse (1989).

local plateau+decline behaviour seen in the  $[\alpha/\text{Fe}] - [\text{Fe}/\text{H}]$  plane. Abundance ratios are recovered and the qualitative behaviour of the  $[\text{Fe}/\text{H}] \sim -0.7$  knee is also seen in the simulated data. The knee-feature seen in Fig. 4 at  $[\text{O}/\text{Fe}] = 0.15$ ,  $[\text{Fe}/\text{H}] = -0.2$  is attributed to the bursty star formation profile which naturally creates multiple knee features as the SNeII:SNeIa rate fluctuates.

Examination of the age distribution (represented by the colour-coding shown in the inset to Fig. 4) reveals rapid early enrichment in  $[\text{Fe}/\text{H}]$ , similar to the age-metallicity relations predicted by classical CE models. Specifically, it takes  $\sim 3$  Gyr to reach a metallicity  $[\text{Fe}/\text{H}] \approx -0.4$ , driven by the initial phases of intense star formation, after which the age-metallicity relation flattens and the rate of growth of  $[\text{Fe}/\text{H}]$  consequently slows (even while SNeIa are becoming more important). This phase is characterised by the abundance ratio ‘strata’ seen in Fig. 4, with discrete ‘arcs’ appearing at decreasing values of  $[\text{O}/\text{Fe}]$  as time progresses.

The influence of the cosmological environment of this simulation is apparent in the abundance patterns of the galaxy. The sub-sample displayed in Fig. 4 exhibits the signature of merger events, e.g. the feature at  $[\text{O}/\text{Fe}] = 0.15$ ,  $[\text{Fe}/\text{H}] = -0.2$ . The full extent of this is only apparent when examining all stars in the galaxy where discrete ‘streams’ with chemical properties distinct from the rest of the galaxy are seen. These arise from accretion of satellites that have lower  $[\text{Fe}/\text{H}]$  values and remain chemically distinct. Larger mergers may have a similar abundance to the primary galaxy but bring gas that can reignite a quiescent galaxy and accelerates the production of Fe in the short term.

## 5 SUMMARY

We present a new chemodynamical simulation code that produces feedback to account for long-lived stars and the elements that they produce. The more sophisticated SN feedback scheme improves the kinematic properties of the stellar fraction (this will be detailed in future work) and gives access to additional constraints on the sub-grid physics. It is clear that the galactic CE for our  $L_*$  galaxy does not perfectly reproduce Milky Way observations, however we believe it serves to demonstrate the validity of this approach. Future work using this code may merit the inclusion of cutting edge nucleosynthesis models (e.g. Doherty et al. 2010) and will make a comprehensive study of the influence of the parameters involved in the underlying CE model.

## 6 ACKNOWLEDGMENTS

The authors thank the referee for their helpful comments. CGF acknowledges the support of the Science & Technology Facilities Council (ST/F007701/1). BKG acknowledges the support of the STFC (ST/F002432/1; ST/G003025/1), Monash University (the Kevin Westfold Distinguished Visitor Programme) and Saint Mary's University. SC acknowledges support from the BINGO Project (ANR-08-BLAN-0316-01) and the CC-IN2P3 Computing Center (Lyon/Villeurbanne, France), a partnership between CNRS/IN2P3 and CEA/DSM/Irfu. DK acknowledges the support of the STFC (ST/H00260X/1). Computing resources were provided by the UK National Cosmology Supercomputer (COSMOS), the University of Central Lancashire's HPC facility and the HPC resources of CINES under the allocation 2010-c2011046642 made by GENCI (Grand Equipement National de Calcul Intensif).

## REFERENCES

- Agertz O., Moore B., Stadel J., Potter D., Miniati F., Read J., Mayer L., Gawryszczak A., Kravtsov A., Nordlund Å., Pearce F., Quilis V., Rudd D., Springel V., Stone J., Tasker E., Teyssier R., Wadsley J., Walder R., 2007, *MNRAS*, 380, 963
- Anders E., Grevesse N., 1989, *Geochim. Cosmochim. Acta*, 53, 197
- Bensby T., Feltzing S., Lundström I., Ilyin I., 2005, *A&A*, 433, 185
- Carbon D. F., Barbuy B., Kraft R. P., Friel E. D., Suntzeff N. B., 1987, *PASP*, 99, 335
- Carigi L., 1994, *ApJ*, 424, 181
- Cayrel R., Depagne E., Spite M., Hill V., Spite F., François P., Plez B., Beers T., Primas F., Andersen J., Barbuy B., Bonifacio P., Molaro P., Nordström B., 2004, *A&A*, 416, 1117
- Chiappini C., Matteucci F., Gratton R., 1997, *ApJ*, 477, 765
- Doherty C. L., Siess L., Lattanzio J. C., Gil-Pons P., 2010, *MNRAS*, 401, 1453
- Dubois Y., Teyssier R., 2008, *A&A*, 477, 79
- Edvardsson B., Andersen J., Gustafsson B., Lambert D. L., Nissen P. E., Tomkin J., 1993, *A&AS*, 102, 603
- Gibson B. K., 1997, *MNRAS*, 290, 471
- Gratton R. G., Carretta E., Claudi R., Lucatello S., Barbieri M., 2003, *A&A*, 404, 187
- Hachisu I., Kato M., Nomoto K., 1999, *ApJ*, 522, 487
- Iwamoto K., Brachwitz F., Nomoto K., Kishimoto N., Umeda H., Hix W. R., Thielemann F., 1999, *ApJS*, 125, 439
- Kawata D., Gibson B. K., 2003, *MNRAS*, 340, 908
- Kobayashi C., 2004, *MNRAS*, 347, 740
- Kobayashi C., Tsujimoto T., Nomoto K., 2000, *ApJ*, 539, 26
- Kodama T., Arimoto N., 1997, *A&A*, 320, 41
- Kroupa P., 2001, *MNRAS*, 322, 231
- Lia C., Portinari L., Carraro G., 2002, *MNRAS*, 330, 821
- Mannucci F., Maoz D., Sharon K., Botticella M. T., Della Valle M., Gal-Yam A., Panagia N., 2008, *MNRAS*, 383, 1121
- Martínez-Serrano F. J., Domínguez-Tenreiro R., Mollá M., 2008, in M. Bureau, E. Athanassoula, & B. Barbuy ed., *IAU Symposium Vol. 245 of IAU Symposium, SPH simulations of the chemical evolution of bulges*. pp 35–36
- Matteucci F., Francois P., 1989, *MNRAS*, 239, 885
- Oppenheimer B. D., Davé R., 2008, *MNRAS*, 387, 577
- O'Shea B. W., Nagamine K., Springel V., Hernquist L., Norman M. L., 2005, *ApJS*, 160, 1
- Pagel B. E. J., Patchett B. E., 1975, *MNRAS*, 172, 13
- Pilkington K., Few C. G., Gibson B. K., Calura F., Michel-Dansac L., Thacker R. J., Molla M., Brook C. B., Stinson G. S., Couchman H. M. P., Bailin J., Wadsley J., 2012, *ArXiv e-prints*
- Pilkington K., Gibson B. K., et al. 2012, *MNRAS*, submitted
- Ramírez I., Allende Prieto C., Lambert D. L., 2007, *A&A*, 465, 271
- Reddy B. E., Lambert D. L., Allende Prieto C., 2006, *MNRAS*, 367, 1329
- Reddy B. E., Tomkin J., Lambert D. L., Allende Prieto C., 2003, *MNRAS*, 340, 304
- Romeo A. D., Portinari L., Sommer-Larsen J., 2005, *MNRAS*, 361, 983
- Sánchez-Blázquez P., Courty S., Gibson B. K., Brook C. B., 2009, *MNRAS*, 398, 591
- Scannapieco C., Tissera P. B., White S. D. M., Springel V., 2005, *MNRAS*, 364, 552
- Shen S., Wadsley J., Stinson G., 2010, *MNRAS*, 407, 1581
- Talbot Jr. R. J., Arnett W. D., 1971, *ApJ*, 170, 409
- Tasker E. J., Brunino R., Mitchell N. L., Michielsen D., Hopton S., Pearce F. R., Bryan G. L., Theuns T., 2008, *MNRAS*, 390, 1267
- Teyssier R., 2002, *A&A*, 385, 337
- Timmes F. X., Woosley S. E., Weaver T. A., 1995, *ApJS*, 98, 617
- Tinsley B. M., 1980, *FCP*, 5, 287
- Tornatore L., Borgani S., Matteucci F., Recchi S., Tozzi P., 2004, *MNRAS*, 349, L19
- Valdarnini R., 2003, *MNRAS*, 339, 1117
- van den Hoek L. B., Groenewegen M. A. T., 1997, *A&AS*, 123, 305
- Wiersma R. P. C., Schaye J., Theuns T., Dalla Vecchia C., Tornatore L., 2009, *MNRAS*, 399, 574
- Woosley S. E., Weaver T. A., 1995, *ApJS*, 101, 181